# Design and Optimisation of Perovskite Plasmonic Nano-laser for operation at room temperature

Swetha Sampath Bobba [a], Nisrine Hamdouni, Kamna Pandey, Kejalakshmy Namassivayane, Arti Agrawal and Kenneth T.V. Grattan [b]

*School of Mathematics, Computer Science & Engineering, City, University of London, Northampton Square, London, EC1V 0HB, United Kingdom*.

(Dated: 4 November 2019)

This work presents the design and optimization of a cascade nano - laser using $CH_3NH_3PbI_3$ perovskite. Due to increasing threshold gain with decreasing device size and high Auger loses, the use of perovskite as the active medium in the cascade nano - laser was proposed, as the material possesses a high emission in the visible wavelength region, with relative ease of device fabrication. By optimizing the thickness of the perovskite, its width and the thickness of the silica used, photonic and plasmonic modes were created which were further considered to permit the generation of lasing, using their respective Purcell Factors. The pump wavelength considered was 400 nm, with laser emission then at 537 nm. For suitability of plasmonic lasing, a Purcell Factor $F_P$ of 1.22 is reported here, with no possibility for photonic lasing due to its $F_P$ value being less than 1 in this design. However, mode crossing effects were observed in the plasmonic mode at $\lambda$ = 400 nm for two designs: at a silica thickness of 27.5 nm with a perovskite thickness and width of 100 nm and 300 nm, and at a silica thickness of 30 nm with a perovskite thickness and width of 95 nm and 300 nm. These mode - crossing effects can further be analysed, to use these devices in the design of potential new sensor systems, mainly for gas and chemical sensing, exploiting the refractive index sensing capability as a means to determine the concentration of the gases, or other chemicals, under study.

## I. INTRODUCTION

Due to their ultra-compact, nanometer size, offering a highly localized coherent output and efficient waveguiding, semiconductor lasers are promising building blocks for nano-scale integrated photonic, plasmonic and other optoelectronic devices [1]. However, with conventional photonic lasers, to generate a light beam on a scale smaller than its wavelength, it is difficult to produce a nano-scale cavity and thus overcome the problems of diffraction limitation. Hence, plasmonic nanolasers [2-6] are a preferred solution for nanoscopic optical applications, compared to the use of conventional lasers.

In a plasmonic nano-laser, the surface plasmons (SP's) at the metal-dielectric interface amplify the input pulse radiation by stimulated emission. These resonant excitations on the micro or nano-scale metal structures tend to form highly localized SPs with large enhancements of the electromagnetic field, also providing good spatial confinement on the sub-wavelength scale. This thereby overcomes the limitations imposed by diffraction. Low temperature plasmonic nano-lasers using different semi-conductor materials such as GaN(Gallium Nitride), CdS(Cadmium Sulphide), or AlGaAs (Aluminum Gallium Arsenide) nanowires have been successfully demonstrated [7-9]. However, these materials are expensive and also require low-temperature operating conditions. Recently, a family of methyl ammonium lead halide perovskites ($CH_3NH_3PbX_3$, where X = I, Br, Cl) and 2D materials such as $MoS_2$ has been reported as one of the promising new materials for photovoltaic technology. This arises because the material possesses excellent coherent light emission properties, due to slow Auger recombination [10-12]. They also have high exciton binding energy, a long exciton diffusion length (in mm) and provide a high fluorescence yield with good wavelength tunability, thereby making them well suited for laser operation.

Zhu et al. have successfully demonstrated such perovskite nano-wire lasers emitting at 777 nm in the near-IR region, with high Q - factor (Quality Factor) and a low threshold (of only 220 nJ/cm$^2$ [13]). In addition, low-threshold perovskite lasers using two-photon optical excitation [14, 15] have also been reported. However, all these nano-laser designs have been constrained to emission below 450 nm and above 680 nm, thereby limiting their potential applications at wavelengths between 450 nm - 680 nm, which importantly includes the absorption region of blood (537 nm - 577 nm) [16]. Such optical sources have potential in the diagnosis and treatment of diseases, including blood and pancreatic cancer taking advantage of high-power radiation in the visible wavelength region.

[a] Electronic mail: swetha.bobba.1@city.ac.uk
[b] Electronic mail: k.t.v.grattan@city.ac.uk

In 2014, Zhang et al. reported a GaN plasmonic nano-laser emitting below 450 nm (and into the ultraviolet region), with an extremely low threshold of 3.5MWcm$^2$ [17].

Plasmonic lasers are constrained by large ohmic and radiation losses, and lasing in them is only achieved either with a high threshold or at low temperatures (from 4K - 120K). Hence, to overcome the limited wavelength bandwidth and low-temperature operating constraints of the existing plasmonic lasers, a cascade nanolaser was designed and optimized at room temperature, using the lead iodine-halide perovskite laser (with a 400 nm pump, which emits at 537 nm), as it exhibits strong and narrow band photoluminescence in the visible wavelength region [13, 18]. These designs are also cost-effective as they can be potentially synthesized on a large scale using a one-step self-assembly method [19], thereby offering a low-cost, room temperature cascaded nano-laser.

## II. LASER DESIGN AND MODAL SOLUTIONS

The laser design consists of three layers arranged in a planar waveguide structure with air as the cladding. Perovskite [20] acts as a gain medium to compensate for the loss in the waveguide. It is deposited over silica and silver substrates to form a dielectric-metal interface, as shown in Figure 1. This metal-dielectric interface generates a plasmonic mode and with the presence of perovskite as a gain medium, a hybrid plasmonic mode in the silica layer was created, using the full vectorial Finite Element Method (FEM) program developed by the authors in FORTRAN [21], as shown in Figures 2 to 4.

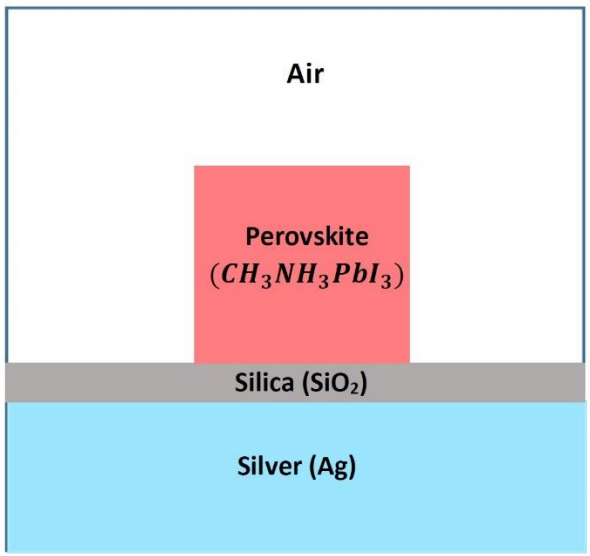


Fig. 1. Ridge waveguide structure of the cascade nano - laser using perovskite as the gain medium, pumping at 400nm and emitting at 537nm.

The device design was further optimized at pump and emission wavelengths of 400 nm and 537 nm respectively, by varying the thickness of the perovskite, H, from 50 nm - 200 nm, its width, W from 100 nm - 400 nm, and the thickness of the silica, d, from 30 nm - 140 nm. This optimization is important because perovskite and silica act as guiding layers for the hybrid plasmonic mode and therefore, optimizing their dimensions increases the mode confinement in these layers, thereby decreasing the propagation loss.

## III. METHODS

The modal solutions for the nano-laser waveguide design shown were obtained using a full vectorial **H**-field formulation, with a penalty term included to eliminate the spurious solution. It is one of the most accurate and numerically efficient approaches to obtain the modal field profiles of a waveguide. Various quasi-TE and quasi-TM modes were calculated from Equation (1) [21], where

$$\omega^2 = \frac{\iint \left[(\nabla \times \mathbf{H})^* \cdot \hat{\varepsilon}^{-1} \cdot (\nabla \times \mathbf{H}) + \left(\frac{\alpha}{\varepsilon}\right)(\nabla \cdot \boldsymbol{H})^* (\nabla \cdot \boldsymbol{H})\right] d\Omega}{\iint \boldsymbol{H}^* \cdot \hat{\mu} \cdot \mathbf{H}\, d\Omega} \quad (1)$$

where **H** is the magnetic field and * denotes a complex conjugate, $\alpha$ is the spurious mode eliminating the penalty term, $\omega^2$ is the eigenvalue, and, $\hat{\varepsilon}$ and $\hat{\mu}$ are the respective permittivity and permeability tensors.

The effective mode area [21] is calculated using the transverse components of magnetic field, F, as,

$$A_{eff} = \frac{\left[\iint_{-\infty}^{+\infty} |F(x,y,\omega)|^2 dx\, dy\right]^2}{\iint_{-\infty}^{+\infty} |F(x,y,\omega)|^4 dx\, dy} \quad (2)$$

and the confinement factor is calculated using [21],

$$\Gamma = \frac{\iint_{\Delta} Re\left(\vec{E} \times \vec{H}^*\right) dx\, dy}{\iint_{\infty} Re\left(\vec{E} \times \vec{H}^*\right) dx\, dy} \quad (3)$$

where $\Delta$ represents the region of interest, and the vectorial $\vec{E}$ and complex conjugate of $\vec{H}(\vec{H}^*)$ fields are used to formulate the modal Poynting vector.

The threshold material gain ($g_{th}$) which is one of the critical factors to decide whether the designed optical device can lase is defined using the photon lifetime ($\tau_p$) and its waveguide confinement factor as [22],

$$g_{th} = \frac{1}{\tau_p v_{g,z}(\omega)\, \Gamma_{wg}} \quad (4)$$

The device design where $\Gamma_{wg}$ is the confinement factor of the waveguide which characterizes the modal gain and $v_{g,z}(\omega)$ is the group velocity of the guided mode given by $v_{g,z}(\omega) \cong \left(\frac{\partial Re[k_z]}{\partial \omega}\right)^{-1}$, calculated using FEM. For efficient lasing, the threshold gain should always be low in units of $\mu m^{-1}$.

The Q factor for a Fabry-Perot mode is defined using the photon lifetime ($\tau_p$), the reflectivity ($R$), the device length ($L$) and the mode resonance frequency ($\omega$) as,

$$Q = \omega\tau_p, where\ \frac{1}{\tau_p} = v_{g,z}(\omega)\left[\alpha_i + \frac{1}{2L}\ln\left(\frac{1}{R^2}\right)\right] \quad (5)$$

The Purcell Factor (FP) is further defined as [23],

$$F_P = \frac{3}{4\pi^2}\left(\frac{\lambda}{n}\right)^3\left(\frac{Q}{V_{eff}}\right) \quad (6)$$

where λ is the wavelength of the material and $V_{eff}$ is the effective mode volume of the cavity.

For a plasmonic mode, the Purcell Factor is defined by the surface plasmon polariton (SPP) waves, radiation modes and lossy surface waves (LSW) as [7, 17],

$$F_P = F_{SPP} + F_R + F_{LSW} \quad (7)$$

where the Purcell Factor for the SPP waves is given by,

$$F_{SPP} = \frac{3}{\pi}\frac{n_g}{n_{perov}}\frac{\left(\frac{\lambda}{2n_{perov}}\right)^2}{A_{eff}}, \quad (8)$$

where the group index, $n_g = \frac{c}{v_g}$ and the group velocity, $v_g = \frac{c}{n_{eff} - \lambda_0\frac{\partial n_{eff}}{\partial\lambda}}$, $n_{perov}$ is the refractive index of the perovskite, λ is the emission wavelength and $A_{eff}$ is the effective mode area of the plasmonic mode obtained using the FEM.

Lossy surface waves are the leaky waves from a metal and their emission rate is defined by the Purcell Factor as,

$$F_{LSW} = \frac{Im\{\varepsilon_m\}\varepsilon_d}{4|\varepsilon_m + \varepsilon_d|^2}\left[\frac{1}{(n_d k_0 h)^3} + \frac{1}{n_d k_0 h}\right] + \left[\frac{Im\{\varepsilon_m\}}{16(n_d k_0 h)}\right] \quad (9)$$

where $\varepsilon_m$ & $\varepsilon_d$ are the permittivity of the metal and dielectric respectively, $n_d$ is the refractive index of the dielectric, $h$ is the thickness of dielectric gain medium and the wavenumber, $k_0 = \frac{2\pi}{\lambda}$. Assuming very small changes in the radiation emission rates, the Purcell Factor of the radiation modes ($F_R$) can be considered as 1.

## IV. RESULTS

By varying the W, H and d of the nano - laser, the variation in modes, complex propagation constant ($\beta$), confinement factor, threshold gain ($g_{th}$) and loss were calculated using the FEM approach. The lasing effect in this nano - laser was further analyzed by calculating the Q - factor and Purcell Factor of the respective modes.

### *A. Variation in Width of Perovskite (W)*

At 400 nm and 537 nm, the value of W was varied from 100 nm – 400 nm with constant values of H = 100 nm and d = 40 nm. The respective $\beta$, CF, $g_{th}$ and loss graphs are plotted in Figure 2.

At 400 nm, from Figure 2a, the propagation of the plasmonic mode becomes constant with increasing W. Also, from Figure 2b, the loss ($= 2\,\beta_i$) decreases sharply from W = 125 nm - 250 nm, with a constant value between W = 300 nm - 400 nm. In addition, as can be seen from Figure 2d, the confinement factor of the plasmonic mode in the silica layer is stable from W = 125 nm – 400 nm. Considering the above parameters - low loss, confinement factor and its corresponding $A_{eff}$ between 0.1 $\mu m^2$ – 0.12 $\mu m^2$ (from Figure 2c), W = 300 nm – 400 nm is considered as the optimum width of the perovskite for the cascade nano - laser design, pumped at 400nm. Figures 2e and 2f represent the dominant $H_x$ - and $E_y$ - field components of the plasmonic mode generated in this laser structure at W = 300nm, H = 100nm and d = 40nm.

At 537 nm, as seen from Figure 2g, the threshold gain for device length where L = 1 μm is constant for W = 250 nm, at an average value of 21 $\mu m^{-1}$. This value however drops to 15 $\mu m^{-1}$ for a device length, L = 10 $\mu m$ for the same value of W. Considering the optimum length of the device for different possible laser applications, threshold gain at L = 1 μm was chosen as the optimum value and as a consequence W = 300 nm – 500 nm, this being the optimum width of the perovskite (also considering its high confinement factor).

A value of W = 300 nm is used for further simulations of the laser design because, at the pump and emission wavelengths (of 400 nm and 537 nm respectively), the threshold gain and other related parameters change negligibly after this value and have a much reduced impact on the design, as seen in Figure 2.

a.

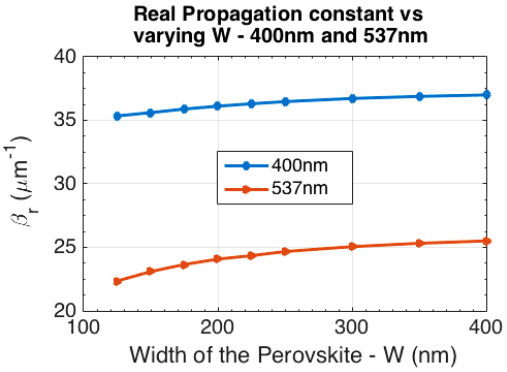


b.

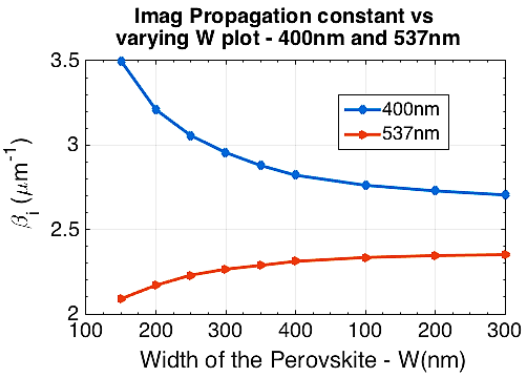

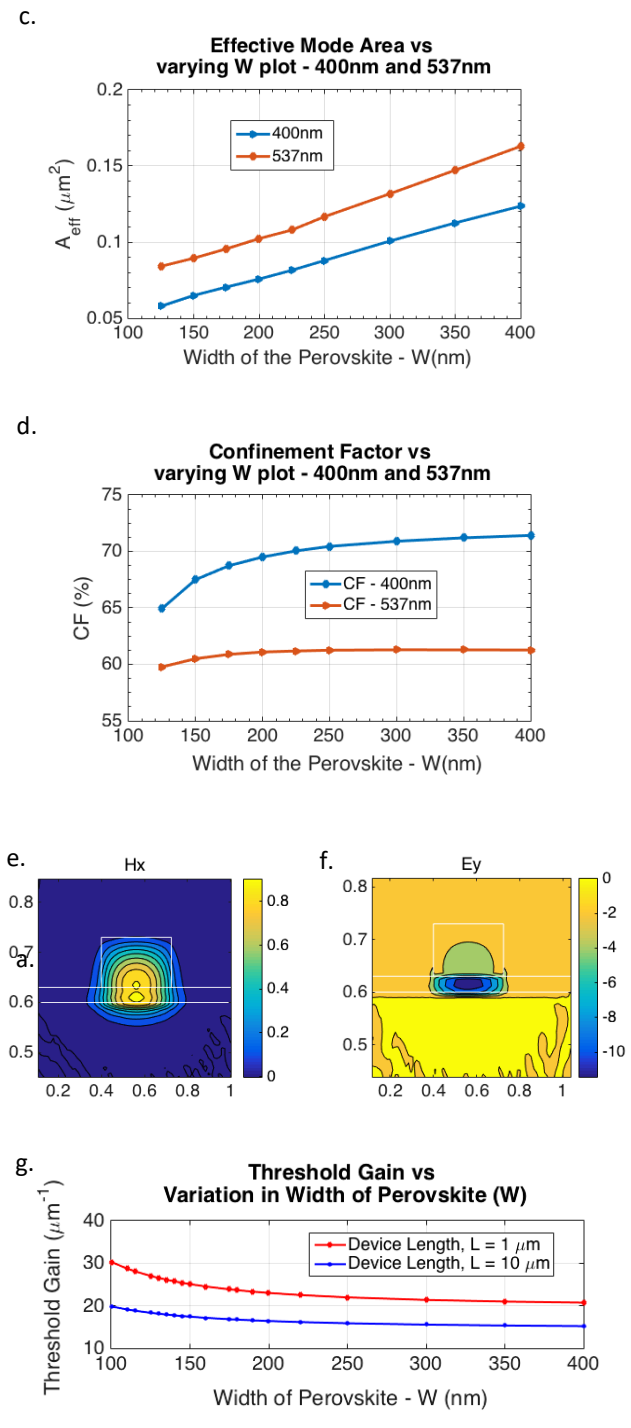


Fig. 2: a, Real propagation constant ($\beta_r$) of the fundamental plasmonic mode ($H_x^{11}$). b, Imaginary propagation constant ($\beta_i$), to calculate the loss. c, Effective mode area ($A_{eff}$) of the $H_x^{11}$ fundamental mode. d, Confinement factor calculated in the guiding silica and perovskite gain layers of the plasmonic mode. e-f, Dominant field components ($H_x$, $E_y$) of the plasmonic mode, with the perovskite nano - laser structure shown in white. g, Threshold gain ($g_{th}$), calculated for variation in width of perovskite (W).

### *B. Variation in Thickness of Perovskite (H)*

With constant values of W and d, as 300 nm and 30 nm respectively, the value of H was varied from 50 nm – 200 nm, this showing mode crossing effects – with plasmonic and photonic mode crossing with each other at a value of H = 95 nm, at a pump wavelength of 400 nm. The complex propagation constant and effective mode area ($A_{eff}$) are calculated and plotted in Figures 3a and 3d, thereby showing this crossing effect at H = 95 nm. Avoiding the mode crossing effect, values of H between 50 nm – 70 nm and 120 nm – 150 nm are considered, to achieve the most suitable thickness of perovskite (H) for the optimum laser design.

At 537 nm, from Figure 3b, the beta imaginary is seen to increase exponentially over H = 100 nm and, from Figure 3c, the confinement factor of silica which is the guiding layer of the plasmonic mode reaches a maximum at H < 90 nm. Figures 3e and 3f represent the dominant $H_x$ - and $E_y$ - field components in the plasmonic nano-laser structure at W = 300nm, d = 30nm and H = 100nm. Using the threshold gain formula from Equation (4) and calculating it with a variation in width and at two device lengths (of 1 µm and 10 µm), it was observed from Figure 3g that the threshold gain is constant for H > 70 nm.

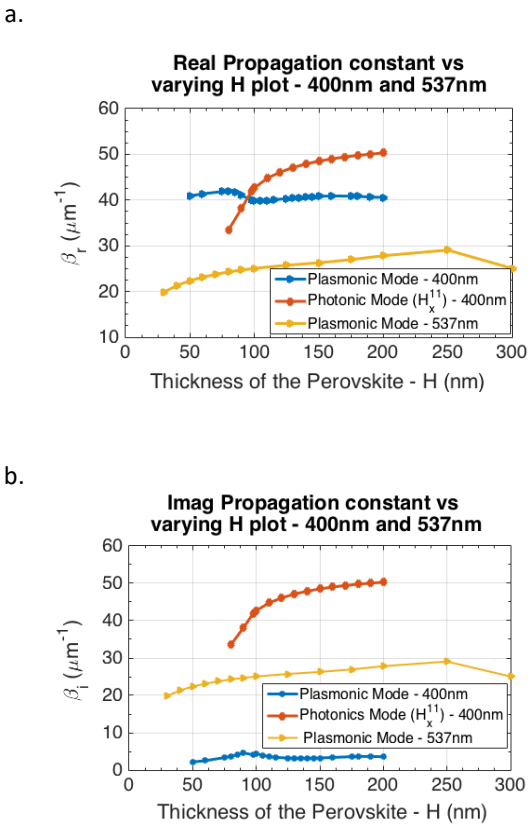

c.

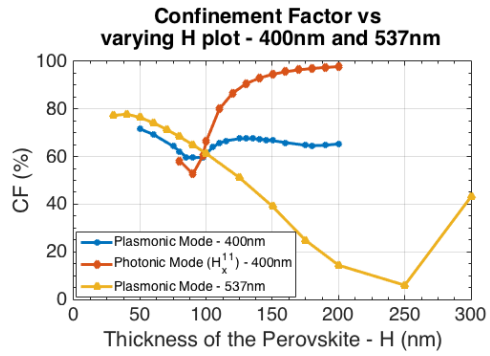


d.

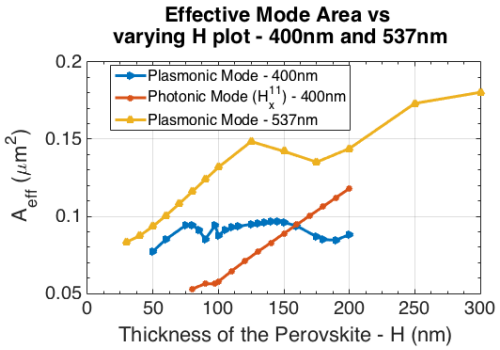


e.

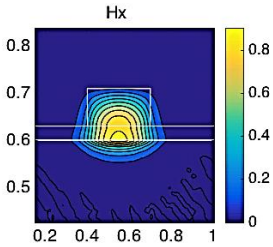


f.

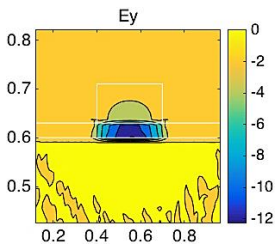


g.

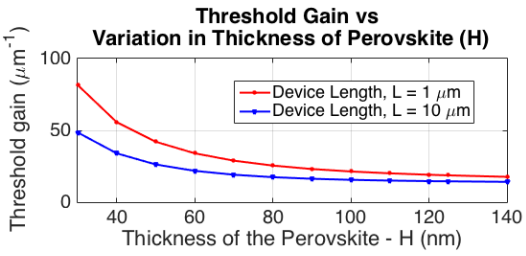


Fig. 3: a, Real propagation constant ($\beta_r$) of the fundamental plasmonic mode ($H_x^{11}$). b, Imaginary propagation constant ($\beta_i$), to calculate the loss. c, Effective mode area ($A_{eff}$) of the $H_x^{11}$ fundamental mode. d, Confinement factor calculated in the guiding silica and perovskite gain layers of the plasmonic mode. e-f, Dominant field components ($H_x$, $E_y$) of the plasmonic mode, with the perovskite nano - laser structure shown in white. g, Threshold gain ($g_{th}$), calculated for variation in thickness of perovskite (H).

Considering all the modal constraints at emission wavelength around 537 nm, with the pump wavelength at 400 nm, H = 100 nm – 120 nm is considered as the optimum thickness range for the perovskite for the cascade nano - laser design studied. This H value thereby avoids the mode crossing effect by still attaining the minimum threshold gain and a low loss, features which are necessary additionally to generate efficient lasing effect in the optimum laser design.

### *C. Variation in Thickness of Silica (d)*

The thickness of silica, d, is now varied over the range from 10 nm – 50 nm with the optimum values of H and W given by 100 nm and 300 nm respectively. Using the FEM, the modal parameters were further calculated (assuming a 400 nm pump wavelength) which showed a mode crossing effect at d = 27.5 nm, for the respective plasmonic and photonic modes of the laser design. This mode crossing effect can be seen from the beta plot in Figure 4a.

From Figure 4d, at 400nm, $A_{eff}$ is low and calculated as between 0.04 µm$^2$ - 0.075 µm$^2$ for d ranging from 10 nm – 25 nm. However, the highest from d = 35 nm – 50 nm with an average waveguide loss of only 3 $\mu m^{-1}$ (from Figure 4b) at this wavelength. From Figure 4c, the confinement in the guiding silica layer is also higher for d > 40nm.

At 537 nm, $A_{eff}$ is linearly increasing with an exponentially decreasing loss. At L = 10 µm, the threshold gain is observed to be constant at a value of d = 25 nm with an average value of 15.5 $\mu m^{-1}$. This has however increased and significantly is constant at a device length, L = 1 µm, over d = 10 nm – 40 nm (shown in Figure 4g).

a.

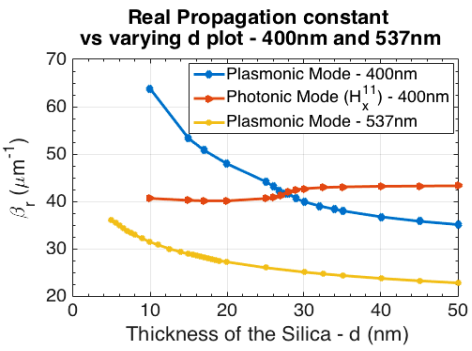

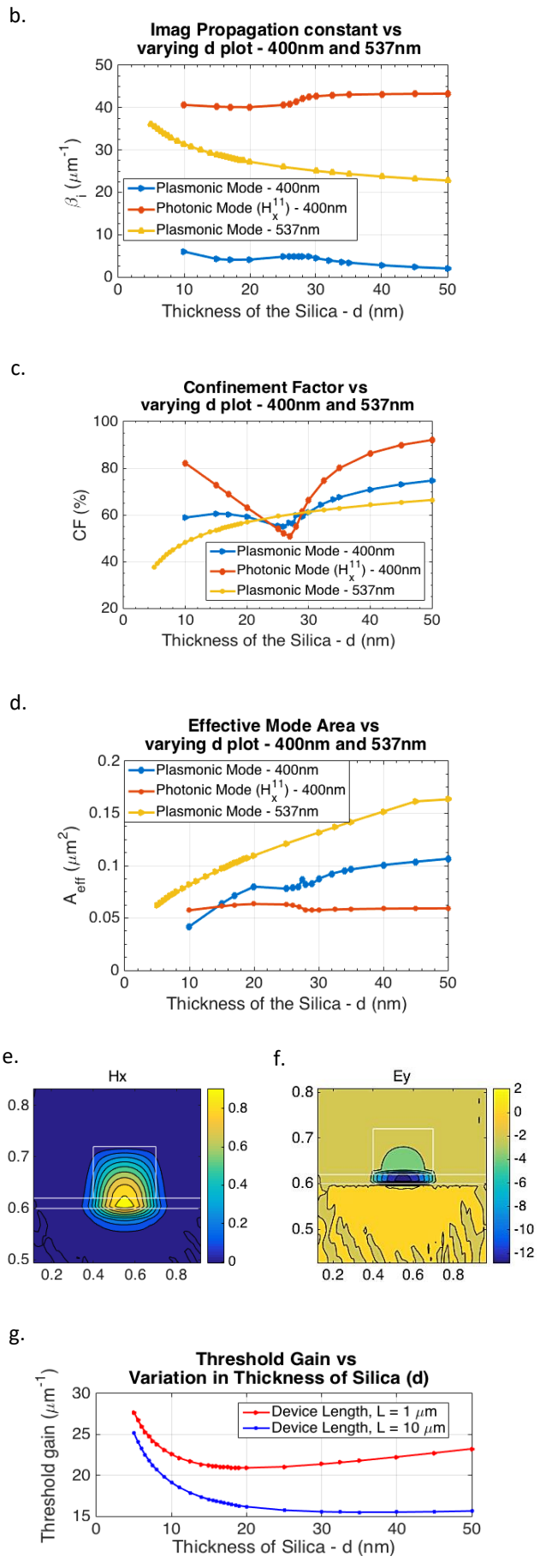


Fig. 4: a, Real propagation constant ($\beta_r$) of the fundamental plasmonic mode ($H_x^{11}$). b, Imaginary propagation constant ($\beta_i$), to calculate the loss. c, Effective mode area ($A_{eff}$) of the $H_x^{11}$ fundamental mode. d, Confinement factor calculated in the guiding silica and perovskite gain layers of the plasmonic mode. e-f, Dominant field components ($H_x$, $E_y$) of the plasmonic mode, with the perovskite nano - laser structure shown in white. g, Threshold gain ($g_{th}$), calculated for variation in thickness of silica (d).

Considering the effective mode area, loss, confinement percentage in the guiding silica layer and threshold gain at both the pump and emission wavelengths of 400 nm and 537 nm, d = 35 nm – 40 nm then becomes the optimum thickness of silica for the cascade perovskite nano - laser design. This thickness also avoids the mode - crossing region at d = 27.5 nm.

*Lasing Phenomenon in the designed Perovskite nano-laser*

Using the respective optimized W, H and d values of 300 nm, 120 nm and 40 nm, the overall Purcell Factor within the $CH_3NH_3PbI_3$ nano - laser was calculated from the sum of the components corresponding to the emission rate of radiation modes ($F_R$), surface plasmon polaritons ($F_{SPP}$) and the lossy surface waves ($F_{LSW}$ ) [17].

The Purcell Factor of the SPP waves was further calculated using Equation (8), where the group velocity ($v_g$) is determined to be 1.4902 x $10^8$ m/s, the group index ($n_g$) is 2.013 and their corresponding $F_{SPP}$ = 0.04353. The extremely localized lossy surface waves associated with the high in - plane momentum leaky waves of the metal are further calculated using Equation (9) as, $F_{LSW}$ = 0.1773. Assuming a small amount of radiation loss, the Purcell Factor for these loses is $F_R$ = 1. The overall Purcell Factor of the plasmonic mode is further calculated using $F_{SPP}$, $F_{LSW}$ and $F_R$ from Equation (7), as $F_P$=1.22.

Ideally, for a device to show laser action, the overall Purcell Factor should be greater than 1 [24] and in this case, this condition is satisfied when $F_P$ = 1.22. Hence, this design of the perovskite nano - laser with the optimized W, H and d values is suitable for lasing on the plasmonic mode. The Purcell Factor for the photonic mode is, however, calculated to be less than 1 (using Equation (6)) and hence, it cannot be used to achieve laser action.

This optimized design could be fabricated [17] by depositing the thin-film silica ($SiO_2$), of thickness 40nm, onto the silver (Ag) substrate using a sputtering technique. The nanometre-scale silica film would be formed initially using plasma-enhanced chemical vapour deposition (PECVD) technology or through the process of thermal oxidation. Perovskite, etched to a thickness of 120nm and width of 300nm would then be deposited onto the $SiO_2$-Ag film substrate to form the optimised nano-laser structure.

## V. CONCLUSION

The design of a perovskite nano - laser has been reported and the design optimized in terms of the width of the perovskite (W) and its thickness (H), as well as that of the silica (d), to avoid the mode - crossing effects and to tailor the design for efficient lasing. Thus, at a pump wavelength of 400 nm and with emission wavelength of 537 nm, using a finite element method (FEM) analysis, both photonic and plasmonic modes could be generated in the proposed nano – laser design.

These modes were further analyzed using the overall waveguide loss ($2\beta_i$), the confinement factor in perovskite (for the photonic mode) and in silica (for the plasmonic mode), and the threshold gain ($g_{th}$) which was calculated for device lengths of 1 µm and 10 $\mu$m respectively, thus to reach optimized values of W, H and d of 300 nm, 120 nm and 40 nm respectively for the laser design put forward. The overall Purcell Factor ($F_P$) for both the photonic and plasmonic modes was evaluated using the emission rates of the SPP waves, the radiation modes and the lossy surface waves which yielded a factor of 1.22 for the plasmonic mode and, 0.11 for the photonic mode.

With $F_P > 1$, the simulation suggests that plasmonic lasing can be exhibited in the perovskite nano - laser, while photonic lasing is not possible since its Purcell Factor is less than 1. Moreover, by using perovskite as the gain medium to compensate for the ohmic and radiation losses, the limitation in the wavelength bandwidth could potentially be overcome by operating at 400nm and lasing at 537nm (in the visible wavelength region), at room temperature. This optimized design thus opens doors to new cost - efficient applications where a nano-laser of this type would prove to be an excellent source.

## REFERENCES


[1] Gu, Q. and Fainman, Y. Semiconductor Nanolasers. (Cambridge University Press, 2017).

[2] Xu, L., Li, F., Liu, Y., Yao, F. and Liu, S., 2019. Surface Plasmon Nanolaser: Principle, Structure, Characteristics and Applications. Applied Sciences, 9(5), p.861.

[3] Jabir, J.N., Ameen, S.M.M. and Al-Khursan, A.H., 2019, July. Ultrahigh Gain from Plasmonic Quantum Dot Nanolaser. In Journal of Physics: Conference Series (Vol. 1234, No. 1, p. 012019). IOP Publishing.

[4] Wu, H., Gao, Y., Xu, P., Guo, X., Wang, P., Dai, D. and Tong, L., 2019. Plasmonic Nanolasers: Pursuing Extreme Lasing Conditions on Nanoscale. Advanced Optical Materials, 7(17), p.1900334.

[5] Oulton, R.F. Surface plasmon lasers: sources of nanoscopic light. Materials Today 15, pp.26-34 (2012).

[6] Wang, S., Chen, H.Z. and Ma, R.M., 2018. High performance plasmonic nanolasers with external quantum efficiency exceeding 10%. Nano letters, 18(12), pp.7942-7948.

[7] Oulton, R.F., Sorger, V.J., Zentgraf, T., Ma, R.M., Glad- den, C., Dai, L., Bartal, G. and Zhang, X. Plasmon lasers at deep subwavelength scale. Nature 461, 629-632 (2009).

[8] Lu, Y.J., Kim, J., Chen, H.Y., Wu, C., Dabidian, N., Sanders, C.E., Wang, C.Y., Lu, M.Y., Li, B.H., Qiu, X. and Chang, W.H. Plasmonic Nanolaser Using Epitaxially Grown Silver Film. Science 337, 450-453 (2012).

[9] Ho J., Tatebayashi J., Sergent S., Fong C. F., Iwamoto S. and Arakawa Y., Low threshold nearinfrared GaAs- AlGaAs core-shell nanowire Plasmon laser. ACS Photon 2, 165-171 (2015).

[10] Hu, F., Yin, C., Zhang, H., Sun, C., Yu, W.W., Zhang, C., Wang, X., Zhang, Y. and Xiao, M. Slow Auger recom- bination of charged excitons in nonblinking perovskite nanocrystals without spectral diffusion. Nano Letters 16, pp.6425-6430 (2016).

[11] Deschler, F. High photoluminescence efficiency and optically pumped lasing in solution-processed mixed halide perovskite semiconductors. The Journal of Phys- ical Chemistry Letters 5, pp.1421-1426 (2014).

[12] Xu, L., Li, F., Wei, L., Zhou, J. and Liu, S., 2018. Design of surface plasmon nanolaser based on MoS2. Applied Sciences, 8(11), p.2110.

[13] H. Zhu, Y. Fu, F. Meng, X. Wu, Z. Gong, Q. Ding, M. V. Gustafsson, M. T. Trinh, S. Jin, and X.-Y. Zhu, "Lead halide perovskite nanowire lasers with low lasing thresholds and high quality factors," *Nature Materials*, vol. 14, no. 6, pp. 636–642, 2015.

[14] Z. Gu, K. Wang, W. Sun, J. Li, S. Liu, Q. Song, and S. Xiao, "Two-Photon Pumped $CH_3NH_3PbBr_3$ Perovskite Microwire Lasers," *Advanced Optical Materials*, vol. 4, no. 3, pp. 472–479, 2015.

[15] Gu, Zhiyuan, *et al.*, "Two-photon pumped lead halide perovskite nanowire lasers." *arXiv preprint arXiv:1510.03987*, 2015.

[16] Bronzino, J.D., Schreiner, S. and Peterson, D.R. Medical Instruments and Devices: Principles and Practices. (CRC Press, 2015).

[17] Q. Zhang, G. Li, X. Liu, F. Qian, Y. Li, T. C. Sum, C. M. Lieber, and Q. Xiong, "A room temperature low-threshold ultraviolet plasmonic nanolaser," *Nature Communications*, vol. 5, no. 1, 2014.

[18] Z.-Y. Zhang, H.-Y. Wang, Y.-X. Zhang, Y.-W. Hao, C. Sun, Y. Zhang, B.-R. Gao, Q.-D. Chen, and H.-B. Sun, "The Role of Trap-assisted Recombination in Lumines- cent Properties of Organometal Halide $CH_3NH_3PbBr_3$ Perovskite Films and Quantum Dots," *Scientific Reports*, vol. 6, no. 1, Jan. 2016.

[19] Q. Zhang, S. T. Ha, X. Liu, T. C. Sum, and Q. Xiong, "Room-Temperature Near-Infrared High-Q Perovskite Whispering-Gallery Planar Nanolasers," *Nano Letters*, vol. 14, no. 10, pp. 5995–6001, Oct. 2014.

[20] S. Luo and W. Daoud, "Crystal Structure Formation of $CH_3NH_3PbI_3$-xClx Perovskite," *Materials*, vol. 9, no. 3, p. 123, 2016.

[21] B. M. A. Rahman and A. Agrawal, Finite Element Modeling for Photonics. Artech House, 2013.

[22] S.-W. Chang and S. L. Chuang, "Fundamental For- mulation for Plasmonic Nanolasers," *IEEE Journal of Quantum Electronics*, vol. 45, no. 8, pp. 1014–1023, 2009.

[23] E. M. Purcell, "Spontaneous Emission Probabilities at Radio Frequencies," *Confined Electrons and Photons NATO ASI Series*, pp. 839–839, 1995.

[24] Baba, T. and Sano, D. Low-threshold lasing and Purcell effect in microdisk lasers at room temperature. IEEE Journal of Selected Topics in Quantum Electronics 9, pp.1340-1346 (200).